Laser Physics Letters

Astro Ltd.

LETTER

Spectral compression in ring similariton fiber laser

To cite this article: Alexei S Abramov *et al* 2019 *Laser Phys. Lett.* **16** 035107

View the article online for updates and enhancements.

IOP ebooks™

Bringing together innovative digital publishing with leading authors from the global scientific community.

Start exploring the collection–download the first chapter of every title for free.

This content was downloaded from IP address 89.239.128.18 on 20/07/2021 at 08:11

IOP Publishing | Astro Ltd
Laser Physics Letters
Laser Phys. Lett. **16** (2019) 035107 (7pp)
https://doi.org/10.1088/1612-202X/ab00fd

Letter

Spectral compression in ring similariton fiber laser

Alexei S Abramov[1], Dmitry A Korobko[1], Igor O Zolotovskii[1] and Andrei A Fotiadi[1,2,3]

[1] Ulyanovsk State University, 42 Leo Tolstoy Street, Ulyanovsk, 432970, Russia
[2] University of Mons, blvd. Dolez 31, Mons, B-7000, Belgium
[3] Aston Institute of Photonic Technologies, Aston University, Birmingham, United Kingdom

E-mail: korobkotam@rambler.ru

Received 20 November 2018, revised 9 January 2019
Accepted for publication 10 January 2019
Published 8 February 2019

Abstract

We present a theoretical model of a ring similariton fiber laser employing nonlinear spectrum compression. A pair of tunnel-coupled optical fibers is used for passive mode-locking. The laser characteristics are simulated for a wide range of laser operation regimes and configuration parameters. The optimized laser system design enables generation of pulses with the maximal efficiency and spectral density providing the lowest losses of energy inside the cavity.

Keywords: spectral compression, similariton fiber laser, laser pulses with high spectral density

(Some figures may appear in colour only in the online journal)

1. Introduction

The laser systems delivering high-energy pulses are of great interest for numerous applications such as material processing, optical communication, medicine, etc. Nowadays, they are among the primary challenges of the fiber laser physics. Mode-locked fiber lasers employing cavities with a high normal dispersion are promising for high energy pulse generation [1–4]. An advance of such lasers in comparison with soliton fiber lasers is a high threshold for operation in multi-pulse regime and, consequently, an order of magnitude higher energy available with single pulse operation (hundreds of pJ to hundreds of nJ) [3–6].

In recent years, the development of high normal dispersion cavity lasers has been driven by the concept of amplifier similariton lasers. A specific feature of these lasers is that the pulses can change their parameters (the pulse spectrum width, duration, energy) drastically as they propagate through the cavity [7, 8]. Such laser dynamics has been demonstrated with both Yb [9, 10] and Er fiber lasers [11, 12]. In this concept, the active fiber could be interpreted as a strong nonlinear attractor, where a short initial pulse is transformed into a parabolic pulse with a linear frequency modulation. A key element of the laser configuration is a spectral filter that narrows the pulse spectrum down to its initial bandwidth after each pulse roundtrip through the cavity, thereby providing a stable similariton generation [13]. The principle drawback of the system is considerable optical energy losses in the filter for high energy pulses that intrinsically possess a broad pulse spectrum. The mechanism of nonlinear spectrum compression (SC) employed in the laser configuration is proposed to overcome this obstacle [14, 15]. The technique is based on compensation of the inverted pulse chirp by self-phase modulation (SPM) in nonlinear fiber with normal dispersion [16–18]. This method provides minimal energy losses in the filter and could be used for development of energy-efficient similariton generators. Similariton lasers employing SC are of great demand as the sources of high spectral density for multiple applications, in particular, in nonlinear optics (multiple harmonics generation, frequency conversion) [19], laser isotope separation [20], etc.

A model of a fiber amplifier similariton laser comprising a spectral compressor has been proposed in [21]. This model

 © 2019 Astro Ltd Printed in the UK

provides the detailed description of amplifier laser operation, but just qualitative description of the passive mode-locking. With careful consideration we found that under given set of parameters the simulation results obtained for the proposed amplifier laser configuration significantly depend on the initial conditions. In particular, the model is not able to describe similariton lasing initiated from the noise level.

In this paper, we apply the amplifier similariton laser model [21] for laser configurations comprising a new kind of all-fiber mode-locking device, thus extending its applicability. As a passive mode-locker, we use a pair of normal dispersion tunnel-coupled fibers (or a twin-core fiber) [22]. Importantly, this element allows mode-locking with a zero relaxation time making the laser description self-consistent and applicable for advanced description of the laser operation. It is worth noting that the proposed technique is similar to the well-known mode-locking mechanism based on nonlinear polarization rotation (NPR) and so could be applied to a variety of fiber similariton laser configurations. The aim of this work is to explore a potential of SC mechanism for generation of pulses with high spectral density of energy. We present numerical simulations describing laser operation in different regimes and wide range of the system parameters.

2. Basic relations

The considered configuration of the ring similariton amplifier laser is shown in figure 1

The optical amplifier (1) is a segment of nonlinear normal group velocity dispersion (GVD) doped fiber. The pulse propagation through the amplifier is described by the complex amplitude $A\,(z,t)$ of the optical wave driven by the nonlinear Schrödinger equation (NSE) [23]

$$\frac{\partial A}{\partial z} - i\frac{\beta_2 - ig/\Omega_g^2}{2}\frac{\partial^2 A}{\partial t^2} + i\gamma_p|A|^2A = \frac{(g-l)}{2}A, \qquad (1)$$

where z is the longitudinal coordinate, t is the time in the running frame, β_2 is the GVD coefficient, γ_p is the Kerr nonlinearity parameter, l is the optical losses, Ω_g is the gain spectrum line width. In our description, the dispersion coefficients of higher orders, nonlinear dispersion and Raman scattering are omitted. This approach is reasonable for the fiber lengths shorter than tens of meters and the pulse duration longer than a few picoseconds. The saturated gain g is

$$g = g_0\left(1 + \frac{1}{E_g}\int |A\,(z,t)|^2 dt\right)^{-1} \qquad (2)$$

where g_0 is the low signal gain and E_g is the gain saturation energy.

The second fiber segment (2) is responsible for passive mode-locking. For this purpose, we use a twin fiber of the length L with a pair of tunnel-coupled optical cores (the coupling coefficient $\sigma = \pi/2L$ [22]). The device is a half-beat-length long so that a low-intensity input in the first arm completely transfers over to the second arm at the exit. A high-intensity pulse can alter the refractive index in the fiber, thereby detuning the coupler and staying in that fiber.

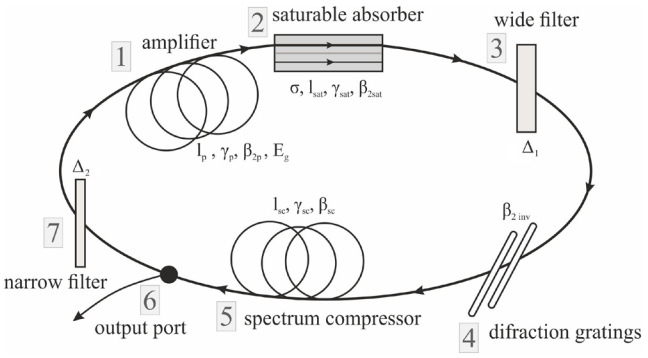

Figure 1. Scheme of the ring similariton generator with nonlinear spectrum compression. The elements: 1—fiber amplifier, 2—saturable absorber, 3—broadband filter A, 4—diffraction gratings, 5—spectral compressor, 6—output coupler, 7—narrowband filter B. Each element is assigned with its parameters.

The radiation propagation in the fibers is described by a set of NSE equations:

$$\frac{\partial A_j}{\partial z} - i\frac{\beta_{2j}}{2}\frac{\partial^2 A_j}{\partial t^2} + i\gamma_j|A_j|^2A_j = i\sigma A_{3-j} - \frac{l_j}{2}A_j, \quad j = 1,2. \qquad (3)$$

The boundary conditions are illustrated in figure 1. The optical signal is introduced into one of the coupled cores ($j = 1$). Radiation from the second core ($j = 2$) is extracted from the cavity. The twin fiber is considered to be symmetrical, so $\beta_{2j} = \beta_{2SA}$ ($\beta_{2SA} > 0$, i.e. dispersions of cores are normal), $\gamma_j = \gamma_{SA}$ and $l_j = l_{SA}$. The dependence of the fiber transmittance on the pulse peak power is similar to that commonly known for passive NPR mode-locking when a configuration 'birefringent fiber' + 'polarization-selective element' [24] is used for the polarized optical radiation. Both mechanisms are similar to saturation absorption. However, in contrast to the real saturable absorbers (SESAMs, carbon nanotubes), they both possess instantaneous response.

The next element is a broadband filter (filter A) (3) used in the configuration to restore envelope of the distorted pulse. The filter bandwidth is a key parameter qualitatively affecting the laser operation regime. Determination of its optimal value is among the primary tasks of this work. It is worth noting that the pulse passing the previous normal dispersion fiber elements acquires a positive frequency modulation due to SPM. For nonlinear SC, a negative frequency modulation has to be imparted to the pulse, i.e. the pulse chirp has to be inverted [16, 17]. A pair of anomalous dispersion diffraction gratings could be employed for this purpose. The anomalous dispersion value β_{inv} could be adopted to minimize distortion of the pulse envelope. Importantly, any decrease of the peak power requires elongation of the SC section. This element is assumed to be linear, so the complex amplitude of the pulse during its propagation varies as

$$\widetilde{A}_{\text{inv}}\,(z,\omega) = \widetilde{A}\,(z,\omega)\cdot\exp\left(\frac{i}{2}\beta_{2\text{inv}}\omega^2\right). \qquad (4)$$

The next fiber section (5, see figure 1) is a passive nonlinear normal GVD fiber used for the SC. As the pulse propagates through this segment, the negative frequency modulation is

Table 1. The ring cavity parameters.

Element	Amplifier					
Parameter	Length l_p (m)	Kerr nonlinearity coefficient γ_p $(\mathrm{W}\times\mathrm{km})^{-1}$	Low signal gain g_0,m^{-1}	GVD,β_{2p} $(\mathrm{ps}^2\ \mathrm{km}^{-1})$	Gain line width (nm)	Gain saturation E_g (J)
Value	6.0	2.5	3.454	5.0	26.75	$0.6\cdot10^{-9}$

Element	Saturable absorbers		Diffraction gratings	Spectral compressor	
Parameter	Coupling strenth (m^{-1})	l_{sat} (m)	$\beta_{2\mathrm{inv}}$ (ps^2)	GVD, β_{sc} $(\mathrm{ps}^2\ \mathrm{km}^{-1})$	Kerr nonlinearity coefficient γ_{sc} $(\mathrm{W}\times\mathrm{km})^{-1}$
Value	0.785	2.0	−0.197	5	2.5

compensated by nonlinear SPM and thus the pulse spectrum is compressed. Then, most of the laser power leaves the cavity through the coupler (element 6). The position of the output coupler is chosen so to generate the pulse with a maximal spectral density of energy. The remaining part of the light is directed to the narrowband filter (filter B) [13] completing the round-trip. In such a way the cycle repeats.

As mentioned above, high optical losses in the filter B are the main drawback of the amplifier similariton laser. The use of SC allows to control the spectrum bandwidth of the generated pulse. Ideally, the spectrum width of the pulse after SC should be narrower than the filter bandwidth. This condition provides the maximal generation efficiency of the similariton amplifier laser. So, with the given values of the gain factor, cavity Q-factor, fiber dispersion and fiber nonlinearity we can define a range, where the other laser parameters have to be optimized to achieve the maximal lasing efficiency and high pulse quality

The fixed system parameters used in the numerical analysis are listed in table 1. We also assume that the output coupler extracts 64% of the laser power from the cavity, the filters possess Gaussian spectrum profiles and all indicated filter bandwidths are FWHM.

3. Numerical analysis

With low-amplitude Gaussian noise used as an initial condition, the laser operation gets stationary regime after 10–15 cavity roundtrips. The pulses exhibit a shape typical for lasers with high normal cavity dispersion: the output pulse duration is 5–10 ps, the pulse spectrum width is 18–37 nm in the range of Yb-doped fiber lasers (1050 nm) and the pulse energy is a few nJ. A specific feature of the similariton laser dynamics is that the pulse bandwidth could vary by more than few orders of magnitude as the pulse propagates through the cavity. Below, we analyze the pulse bandwidth evolution and study how the laser pulse characteristics change with the laser system parameters.

Let us consider the dependence of the spectral compression quality (evaluated as a ratio of line widths $\Delta/\Delta_{\mathrm{comp}}$ before and after SC) and the output pulse energy on the bandwidth of the filter A Δ_1. These dependences are shown in figure 2 for the filter bandwidth varying in the range (14..35) nm. In this case, the bandwidth of filter B is assumed to be constant and

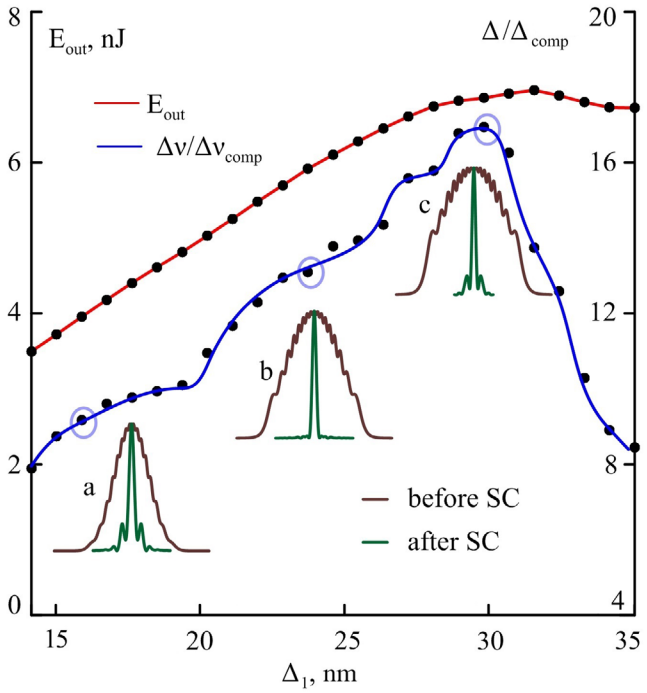

Figure 2. The red line: dependence of the output pulse energy on the bandwidth of filter A. The blue line: dependence of the spectrum compression quality on the bandwidth of the filter A. The insets show the spectra before (brown) and after compression (green) at the bandwidth of filter A of $\Delta_1 = (16\ (\mathrm{a}), 24\ (\mathrm{b}), 30\ (\mathrm{c})$ nm).

equal to $\Delta_2 = 0.9$ nm. Figure 2 shows that with an increase of the filter A bandwidth up to $\Delta_1 = 30$ nm the output pulse energy increases almost linearly. With a further increase of Δ_1, the dependence of the pulse energy on this parameter disappears as the filter A bandwidth becomes wider than the pulse spectrum width.

The compression quality of the pulse spectrum also strongly depends on the bandwidth of the filter A. For a relatively narrowband filter $\Delta_1 < 17.5$ nm, the SC ratio is less than 10–12. With an increase of the filter bandwidth, the compression ratio increases and the pulse spectrum broadens as well. However, with the filter A bandwidth higher than $\Delta_1 > 30$ nm, the compression quality drops rapidly. The insets in figure 2 show the pulse spectra before and after compression for the selected filter bandwidths $\Delta_1 = 16$ nm (a), $\Delta_1 = 24$ nm (b) and $\Delta_1 = 30$ nm (c). Here, the SC element length is adopted for

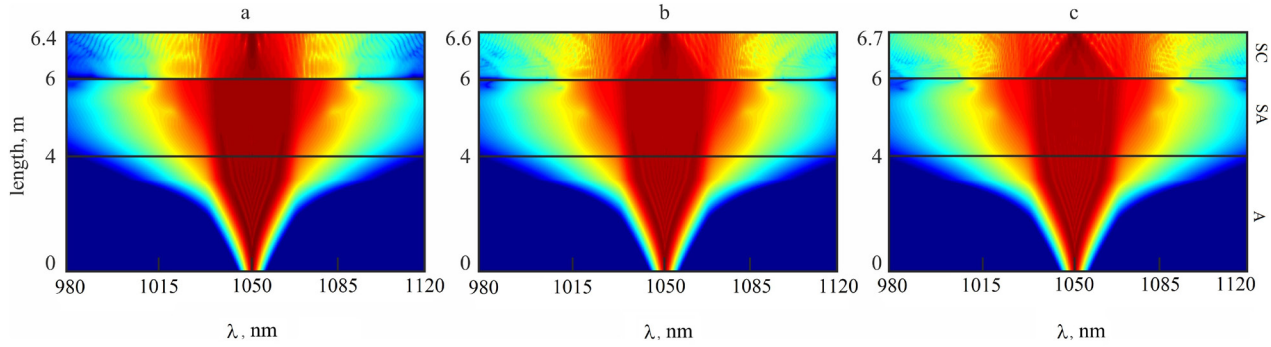

Figure 3. Pulse spectrum evolution inside the cavity. The filter A bandwidth $\Delta_1 = (16\ (a), 24\ (b), 30\ (c)$ nm (a)–(c)). A-amplifier, SA-saturable absorber, SC-spectrum compressor, uneven Y scale.

each value of $\Delta\nu_1$ to provide the best compression. The insets show the pulse spectrum compression quality at different Δ_1.

The parabolic pulse possessing a linear frequency modulation (chirp) is known to be the most suitable for nonlinear SC [17, 25, 26]. In our case, the pulse shape and its spectrum vary significantly during pulse propagation inside the cavity (figure 3). At the first stage, as the pulse propagates through the amplifying segment of the cavity, the Gaussian pulse shape with a narrow spectral width transforms into a frequency-modulated pulse with a shape close to a parabola (with the gain line and saturation energy $\Omega_g, E_g \to \infty$ the pulse shape asymptotically approaches parabola). Then, as the pulse propagates through the twin fiber (the saturable absorber), the pulse shape distorts. One can see that with the filter A bandwidth of $\Delta_1 < 20$ nm the pulse exhibits Gaussian shape. However, after distortion caused by SC undesired sidebands are generated (inset 'a' in figures 2 and 3). At $\Delta_1 > 27$ nm, filter A fails smoothing the pulse distortions induced by the saturable absorber or caused by nonlinear frequency modulation associated with the finite gain line width Ω_g. As a result, undesirable sidebands (inset c) are also formed in the pulse spectrum during the SC stage and the compression quality decreases. Thus, for the used fixed system parameters, the best laser operation is observed when the bandwidth of the first filter is within the frequency range of $\Delta_1 = (20..27)$ nm (inset (b)). The pulse shape and pulse chirp are closest to the most suitable for SC thus providing the output pulse spectrum of the best quality.

Let us analyze the dependence of the SC quality and the pulse energy loss in filter B ΔE on the bandwidth of this filter Δ_2 (figure 4). The bandwidth of filter A is kept fixed $\Delta_1 = 24$ nm within the range of optimal compression. The bandwidth of filter B varies within the range of $\Delta_2 = (0.7..14)$ nm divided into three conventional domains. Within the first domain, the filter B bandwidth is quite narrow and the energy losses caused by the filter are high enough (inset (a)). These losses depend not only on the filter B bandwidth but also on the filter A bandwidth Δ_1. Decrease of Δ_1 is accompanied by distortions during the SC and, hence, an increase of optical losses in filter B. The compression quality depends significantly on the filter B bandwidth $\Delta\nu_2$. The filter B with extremely narrow bandwidth $\Delta_2 = 0.7$ nm transits only small part of the pulse energy into the active fiber. As a result, the acquired pulse chirp is significantly lower than

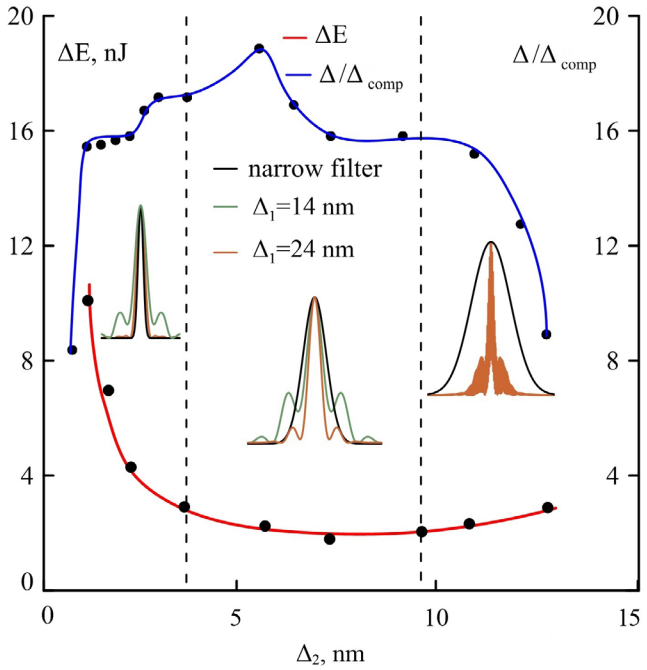

Figure 4. Red line: the dependence of the pulse energy loss in narrowband filter B on the bandwidth Δ_2. Blue line: the dependence of the pulse compression quality on Δ_2.

the asymptotic value typical for parabolic similariton [27], i.e. due to insufficient spectrum broadening during the amplification the compression quality is low. One can see that even a small increase of Δ_2 can significantly increase the pulse spectrum broadening and compression degree. With a further increase of Δ_2, the energy losses also decrease, but within the second domain the optical loss level just slightly depends on the filter B bandwidth (inset (b)). The best degree of SC close to 20 is achieved (at $\Delta_2 \approx 5.5$ nm) in this domain.

A further increase of the filter B bandwidth leads to significant spectral distortions and appearance of parasitic sidebands. In the third domain $\Delta_2 > 9$ nm, the laser system starts to operate multi-pulses. The corresponding spectrum exhibiting a characteristic fringe structure is shown in figure 2(c). This regime is characterized by significant deterioration of the compression quality and growth of energy losses in filter B. This can be explained by the following mechanism. During the pulse amplification the pulse spectrum width increases

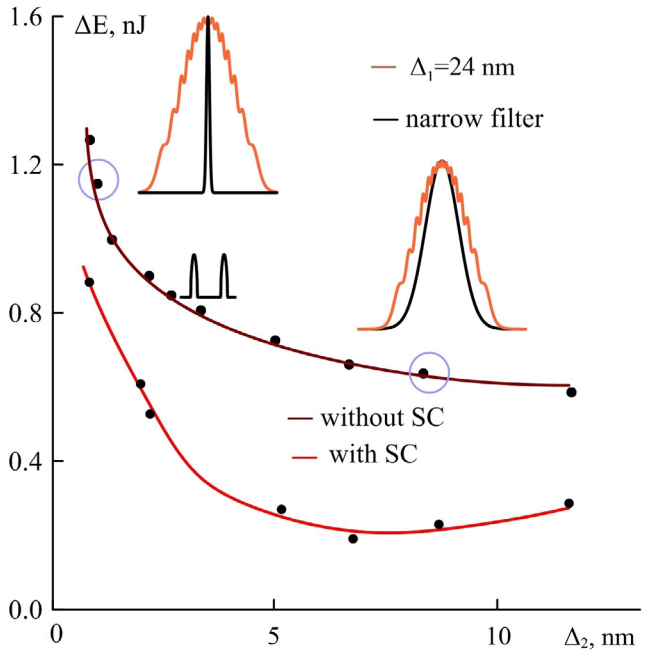

Figure 5. Dependence of energy losses in filter B on its width for laser configurations with (red line) and without (brown line) SC. Insets show the pulse spectra (brown) obtained at the filter B input for $\Delta_1 = 24$ nm in comparison with the filter B spectrum (black).

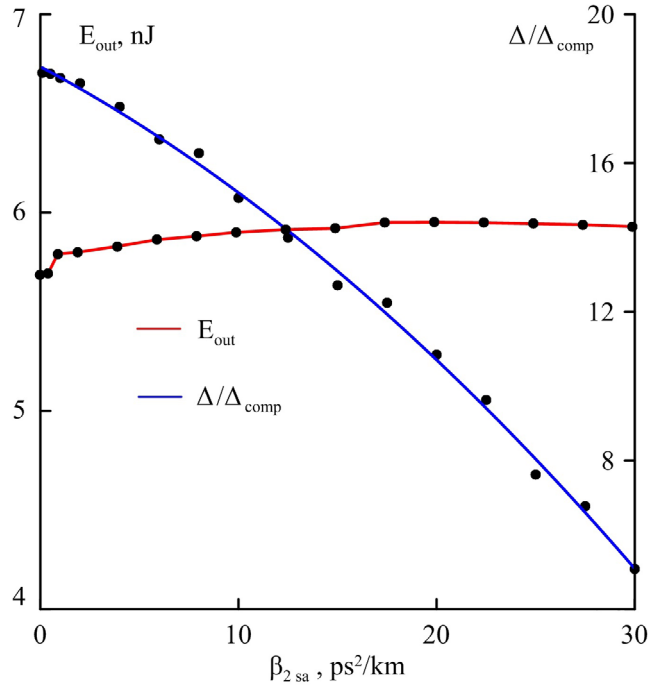

Figure 6. Dependence of the output pulse energy (red line) and SC quality (blue line) on the saturable absorber GVD.

due to SPM up to values exceeding the limited width of the gain line thus providing a negative feedback. The pulses with higher energy suffer stronger losses and generation of extra pulses inside the cavity is energetically reasonable. Therefore, the narrowband filter B, a key element in amplifier similariton laser configuration, is also very important for the laser system employing nonlinear SC. The optimal bandwidth of the filter should belong to the range of 3.5 nm $< \Delta_2 <$ 5.5 nm providing a relatively high degree of compression in combination with low energy losses.

To analyze the energy efficiency of the considered configuration, we evaluate the optical losses in the laser configuration without spectral compression. The broadband filter A bandwidth is fixed at $\Delta_1 = 24$ nm. Figure 5 shows the dependences of the energy losses in filter B ΔE on this filter bandwidth in the system with (red curve) and without (brown line) the SC element.

One can see that SC reduces energy losses by several (2–3) times thereby increasing the efficiency of the similariton generation. The maximal laser efficiency is achieved for the filter B bandwidth that corresponds to the best compression quality (at $\Delta_2 \approx 5.5$ nm). Noteworthy, in the absence of SC, a stable single-pulse generation regime is obtained for low $\Delta_2 < 1.75$ nm only. For larger bandwidths, generation of two pulses of low energy is energetically more reasonable in the laser without SC leading to multi-pulsing. Therefore, we can conclude that the nonlinear SC element used in a similariton laser configuration causes not only reduction of optical losses but also increases the maximal output pulse energy.

Further, let us analyze the effect of saturable absorber characteristics (GVD and nonlinearity in the twin fiber) on the laser generation. The bandwidths of the filters are fixed at $\Delta_1 = 24.5$ nm and $\Delta_2 = 0.9$ nm. Figure 6 demonstrates the dependence of the compression quality and the output pulse energy on the GVD in the saturable absorber. The pulse energy just weakly depends on this parameter. However, the SC quality, in contrast, strongly depends on the saturable absorber dispersion. Therefore, for better spectrum compression the GVD has to be minimized. These effects are explained by dispersive spreading of the pulse during its propagation in the saturable absorber that causes approaching of the pulse envelope to the Gaussian shape resulting in an increase of its duration and peak power decrease. Deviation of the envelope from the optimal shape leads to a decrease of the SC quality. Dispersion effects in saturable absorber do not change the pulse spectrum width. Therefore, the pulse energy is maintained as the pulse passes through the filters and spectral compressor.

The effect of the saturable absorber nonlinearity on characteristics of the generated pulses is shown in figure 7. The nonlinearity significantly affects the compression quality that degrades linearly with an increase of γ_{SA}. Noteworthy, the saturable absorber nonlinearity limits the peak power of the generated pulses. The nonlinear phase shift $\sim \gamma_{SA}|A|^2 l_{SA}$ at the saturable absorber transmission maximum is fixed. Getting the maximum, the saturable absorber transmission coefficient keeps high value during the induced increase of nonlinearity only if the peak power of a single pulse decreases. As a result, the pulse energy decreases and the optical losses are released through the coupled fiber (domain (a) in figure 7 corresponds to low nonlinearities $\gamma_{SA} = (2..8)\ (W \cdot km)^{-1}$).

With an increase of nonlinearity and phase shift up to a certain threshold, the appearance of a new pulse in the cavity becomes energetically preferable, i.e. like in previous cases, the losses of two pulses passing through the cavity are lower

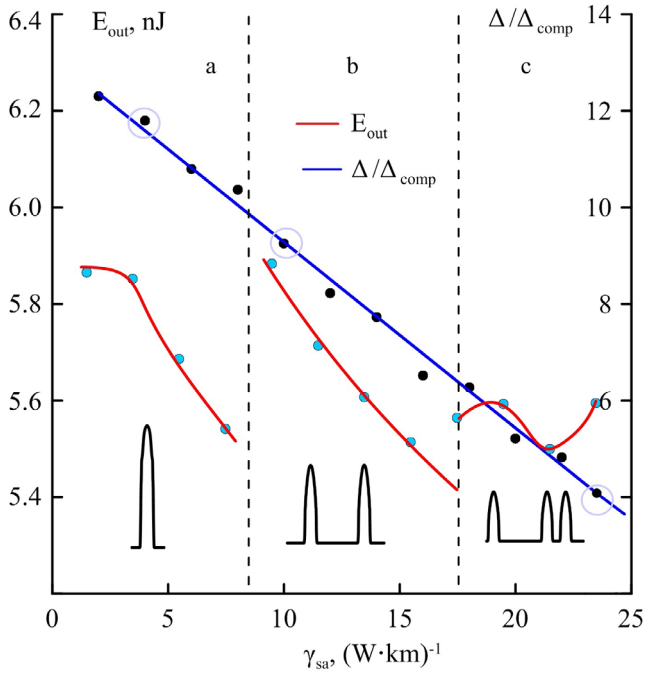

Figure 7. Dependence of the output pulse energy (red line) and degree of SC (blue line) on the saturable absorber nonlinearity. Insets: the temporal pulse shapes obtained for $\gamma_{SA} = 4\ (W \cdot km)^{-1}$ (a), $\gamma_{SA} = 10\ (W \cdot km)^{-1}$ (b) и $\gamma_{SA} = 22\ (W \cdot km)^{-1}$ (c).

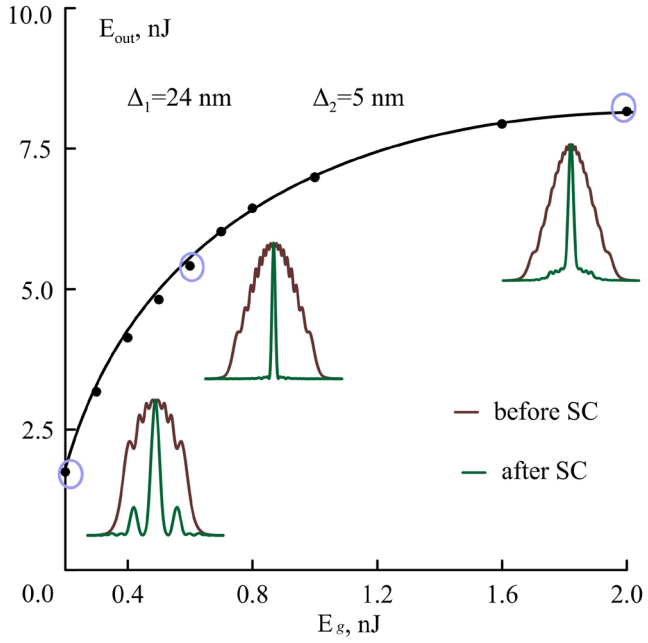

Figure 8. Dependence of the output pulse energy on the gain saturation energy E_g. The insets show the spectra before (brown) and after compression (green) at the value of $E_g = (0.2, 0.6, 2.0$ nJ).

than those observed for one pulse of higher energy. After transition processes including gain competition, the energies and powers of pulses are equalized. Thus, nonlinearity increase causes transition of the laser to generation of two (domain (b)) and three (domain (c)) pulses inside the cavity. Decrease of the SC quality can be attributed to the decrease of the maximal pulse bandwidth in the cavity.

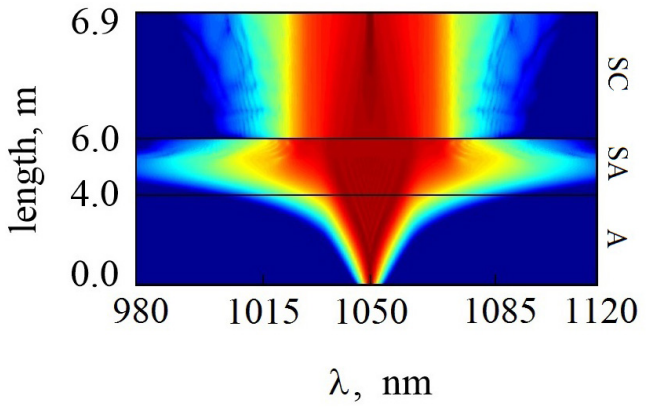

Figure 9. Pulse spectrum evolution inside the cavity. The filter bandwidths are $\Delta_1 = 24$ nm, $\Delta_2 = 5$ nm, $E_g = 0.8$ nJ. A-amplifier, SA-saturable absorber, SC-spectrum compressor.

Finally, we consider the dependence of the output pulse energy on the gain in the active fiber. For this purpose, we fix the filter bandwidths as $\Delta_1 = 24$ nm $\Delta_2 = 5$ nm, values of the other parameters are the same as in modeling of figures 2–5 (table 1). The gain value is changed by varying the gain saturation energy $E_g = (0.2..2)\ nJ$ with constant law signal gain g_0. The simulation results presented in figure 8 show the dependence of the output pulse energy on E_g. The insets show the pulse spectra before and after compression for the selected value of the gain saturation energy. One can see that the gain value affects the pulse shape and its spectrum. At small E_g, undesired sidebands are generated in the pulse spectrum after distortion caused by SC. With increasing gain, the spectrum approaches the parabolic shape providing destruction of these sidebands but the increase in output pulse energy is reduced due to filtering. At high values of E_g, the pulse energy is nearly independent of the gain due to strong filtering. So one can conclude that the optimal laser efficiency is reached in the range of $E_g = (0.5..1)\ nJ$. The pulse spectrum evolution for $E_g = 0.8$ nJ is shown in figure 9.

4. Conclusion

In this paper, we have presented extended numerical simulations of an amplifier similariton fiber laser employing nonlinear SC. It is shown that the high energy output pulses demonstrate high degree of SC for a wide range of filter bandwidths. Tuning of the filter bandwidth allows to increase the energy efficiency of pulse generation in the laser and to obtain the output pulses of much higher energy than in the system without SC. The output pulses of high spectral density are attractive not only due to their multiple nonlinear optics applications but also due to their suitability for further amplification. Indeed, the limited gain line width of optical systems is one of the main limiting factors in generation of high energy pulses. The use of the proposed laser as a source of high-power spectrally dense pulses could enable a drastic increase of the output pulse maximal energy and generation efficiency in high-power laser systems. Additionally, we should note that novel optical processing technologies enabling pulse

formation with the given envelope profile and frequency modulation are considered as a way to increase the laser efficiency and decrease losses during the pulse generation. Programmable liquid crystal phase masks and acousto-optical filters are among such advanced elements [28–30]. Therefore, the results on the pulse spectrum management described in this paper could be considered in this context.

Also, we have applied the theory of a similariton generator to the laser configuration employing mode-locking mechanism based on tunnel-coupled nonlinear fibers. The effect of fiber dispersion parameters and nonlinearity on characteristics of the generated pulses has been studied. The analogy between mode-locking mechanisms proposed in this paper and commonly used nonlinear polarization rotation mechanism allows to apply the results obtained here for a wide range of fiber laser configurations considered earlier (employing normal cavity dispersion and nonlinear spectrum compression), thereby extending the range of application of the discussed mechanism.

Acknowledgments

The work is supported by the Russian Scientific Foundation (project 16-42-02012), the Russian Foundation for Basic Research (project 16-42-730084) and the Ministry of Education and Science of the Russian Federation (project 3.3889.2017/4.6). AAF acknowledges the Leverhulme Trust (UK) for his Visiting Professorship (VP2-2016-042).

References

[1] Fu W, Wright L G, Sidorenko P, Backus P and Wise F W 2018 *Opt. Express* **26** 9432–63
[2] Renninger W H, Chong A and Wise F W 2008 *Opt. Lett.* **33** 3025–7
[3] Chong A, Renninger W H and Wise F W 2007 *Opt. Lett.* **32** 2408–10
[4] Ruehl A, Kuhn V, Wandt D and Kracht D 2008 *Opt. Express* **16** 3130–5
[5] Wise F W, Chong A and Renninger W H 2008 *Laser Photon. Rev.* **2** 58–73
[6] Lecaplain C, Chédot C, Hideur A, Ortaç B and Limpert J 2007 *Opt. Lett.* **32** 2738–40
[7] Chong A, Wright L G and Wise F W 2015 *Rep. Prog. Phys.* **78** 113901
[8] Zolotovskii I O, Korobko D A and Stoliarov D A 2016 *Quantum Electron.* **46** 1092
[9] Renninger W H, Chong A and Wise F W 2010 *Phys. Rev.* A **82** 021805
[10] Nie B, Pestov D, Wise F W and Dantus M 2011 *Opt. Express* **19** 12074–80
[11] Krylov A A, Sazonkin S G, Lazarev V A, Dvoretskiy D A, Leonov S O, Pnev A B and Dianov E M 2015 *Laser Phys. Lett.* **12** 065001
[12] Tang Y, Liu Z, Fu W and Wise F W 2016 *Opt. Lett.* **41** 2290–3
[13] Bale B G and Wabnitz S 2010 *Opt. Lett.* **35** 2466–8
[14] Stolen R H and Lin Q 1978 *Phys. Rev.* A **17** 1448–53
[15] Limpert J P, Gabler T, Liem A, Zellmer H and Tünnermann A 2002 *Appl. Phys.* B **74** 191–5
[16] Andresen E R, Dudley J M, Oron D, Finot C and Rigneault H 2011 *Opt. Lett.* **36** 707–9
[17] Fatome J, Kibler B, Andresen E R, Rigneault H and Finot C 2012 *Appl. Opt.* **51** 4547–53
[18] Korobko D A, Okhotnikov O G and Zolotovskii I O 2016 *J. Opt. Soc. Am.* B **33** 239–45
[19] Wynands R, Coste O, Rembe C and Meschede D 1995 *Opt. Lett.* **20** 1095–7
[20] Makarov G N 2015 *Phys.—Usp.* **58** 670–700
[21] Boscolo S, Turitsyn S K and Finot C 2012 *Opt. Lett.* **37** 4531–3
[22] Walton D T and Winful H G 1993 *Opt. Lett.* **18** 720–2
[23] Agrawal G P 2007 *Nonlinear Fiber Optics* 4th edn (Berlin: Springer)
[24] Chen C J, Wai P K A and Menyuk C R 1992 *Opt. Lett.* **17** 417–9
[25] Finot C and Boscolo S 2016 *J. Opt. Soc. Am.* B **33** 760–7
[26] Abramov A S, Zolotovskii I O, Korobko D A and Fotiadi A A 2018 *Opt. Spectrosc.* **124** 343–8
[27] Dudley J M, Finot C, Richardson D J and Millot G 2007 *Nat. Phys.* **3** 597–603
[28] Boscolo S, Finot C, Karakuzu H and Petropoulos P 2014 *Opt. Lett.* **39** 438–41
[29] Zolotovskii I O, Korobko D A, Sysoliatin A A and Fotiadi A A 2016 *J. Russ. Laser Res.* **37** 448–58
[30] Monmayrant A, Weber S and Chatel B 2010 *J. Phys. B: At. Mol. Opt. Phys.* **43** 103001